Structure and formation of $H_2Ti_3O_7$ nanotubes in an alkali environment

S. Zhang, Q. Chen, and L.-M. Peng*
Key Laboratory on the Physics and Chemistry of Nanodevices and Department of Electronics, Peking University, Beijing 100871, China
(Received 18 June 2004; revised manuscript received 11 October 2004; published 4 January 2005)

The structure and growth of $H_2Ti_3O_7$-type nanotubes have been studied by first-principle calculations. It is shown that the asymmetry in the distribution of hydrogen on the two sides of the surface layer of a $H_2Ti_3O_7$ crystal plate provides a sufficient driving force for the formation of the $H_2Ti_3O_7$ nanotube. Hydrogen deficiency on one side of the surface layer of a $H_2Ti_3O_7$ plate results in a surface tension that increases with increasing hydrogen deficiency and may eventually overcome the coupling from the layers beneath driving the surface layer to peel off from the crystal plate and roll into a tubular structure. While the radius of the resultant nanotube is determined mainly by the layer coupling energy, the thickness of the tube wall is determined by the residual charges on the peeled surface layer. Both the radius and the wall thickness may in principle be controlled via modifying the layer coupling strength and the net charges on the surface.

DOI: 10.1103/PhysRevB.71.014104 PACS number(s): 61.46.+w, 68.37.Lp, 77.84.Dy

I. INTRODUCTION

Since the discovery of carbon nanotubes by Iijima in 1991,[1] these materials have been extensively studied due to their exceptional electric, mechanical, and chemical properties. Various nanotubes have since been synthesized, including BN,[2] $B_xC_yN_z$,[3] WS_2,[4] MoS_2,[5] $W_xMo_yC_zS_2$,[6] VO_x,[7] and TiO_2 (Refs. 8 and 9) nanotubes. Very recently Du *et al.*[10] found that trititanate nanotubular materials may be obtained via a simple alkali treatment of TiO_2 particles in NaOH aqueous solution. These nanotubular materials were later determined to be nanotubes of the $H_2Ti_3O_7$.[11,12]

The synthetical procedure of the $H_2Ti_3O_7$-type nanotubes is relatively simple. In a typical synthesis TiO_2 particles (either pure anatase phase or mixed anatase and rutile phases) with particle size ranging from 10 nm to more than 200 nm were added in a 10-M NaOH acqueous solution. The specimen was sealed in a Teflon container and statically heated in a furnace at 130 °C for 72 h. The final white product was filtered and washed at room temperature with different solvents, including water, ethanol, and acetone, and a large quantity of nanotubes (with a yield $>90\%$) were obtained. These experiments suggest that the washing solvents have hardly any effects on the product. It was therefore concluded that the $H_2Ti_3O_7$-type nanotubes were formed during the alkali treatment of the TiO_2 particles, i.e., in the NaOH solution.

Comprehensive transmission electron microscopy (TEM) observations revealed that at a very early stage, TiO_2 particles reacted with NaOH solution and a highly disordered intermediate phase containing Ti, O, and Na was formed. Shown in Fig. 1 is a TEM image obtained from a product after the TiO_2 particles reacted with the NaOH solution for half a day. The product is seen to be composed of mainly the intermediate phase (the dark region to the right of the figure) and whiskers extruded from this phase. After three days, most of these whiskers became nanotubes with uniform diameter, and the main by-products were crystalline $H_2Ti_3O_7$ plates.[11] Shown in Fig. 2(a) is a TEM image showing both the nanotubes (in the region marked by T) and $H_2Ti_3O_7$ crystal plates (in the region marked by P). Shown in Fig. 2(b) is an enlarged image of region T, and in Fig. 2(c) is an enlarged image of region P. The tubular materials shown in Fig. 2(b) were determined to be of the $H_2Ti_3O_7$-type.[11,12] Detailed measurements were made on the outer and inner diameters of these nanotubes and the results are summarized in Fig. 3. These histograms show that the $H_2Ti_3O_7$-type nanotubes are distributed narrowly around 6–8 nm (average diameter), and typically the tubes are multiwall nanotubes having four shells.

Figure 2(c) shows both nanotubes (marked by T) and crystal plates, and a high-resolution TEM image of these plates is shown in Fig. 4. These crystalline plates are indeed $H_2Ti_3O_7$ plates. It was proposed that these sheets of trititanate may extrude from the disordered phase as shown in Fig.

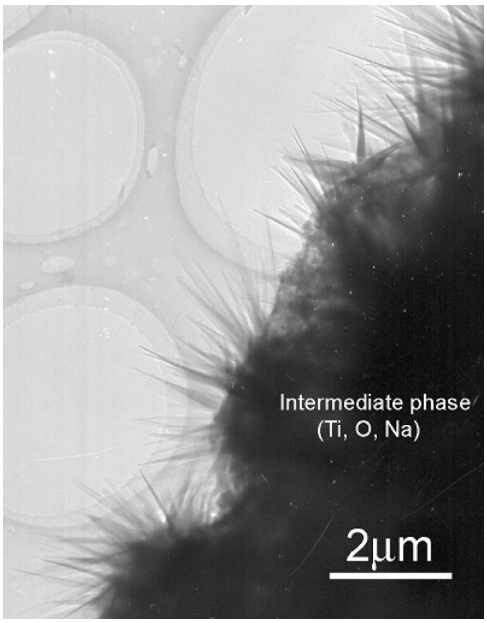

FIG. 1. A low magnification TEM image showing the formation of a disordered intermediate phase containing Ti, O and Na and the growth of whiskers from this intermediate phase after TiO_2 reacted with NaOH solution for about half a day.

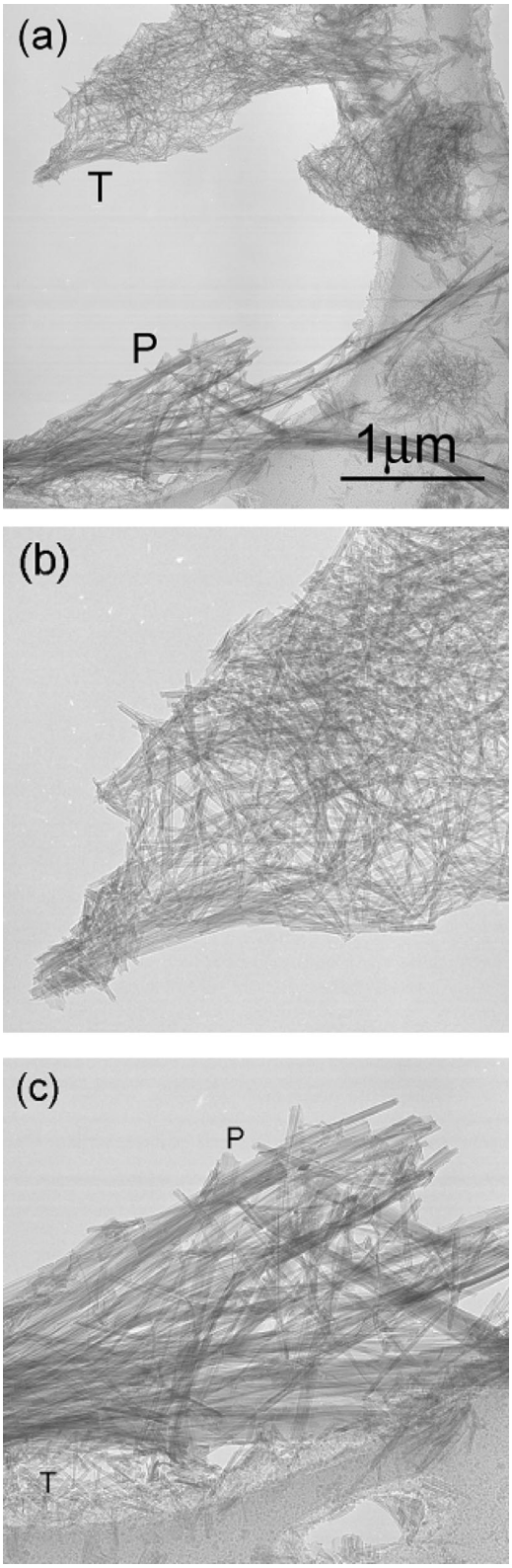

FIG. 2. TEM images showing the product after TiO_2 particles reacted with NaOH solution for one day. In (a) is a low magnification TEM images showing that the product is composed of mainly nanotubes and crystal plates. Shown in (b) is an enlarged image of region T as marked in (a), and in (c) is that of region P. In (c) both crystal plates and nanotubes are visible in regions marked by T and P, respectively.

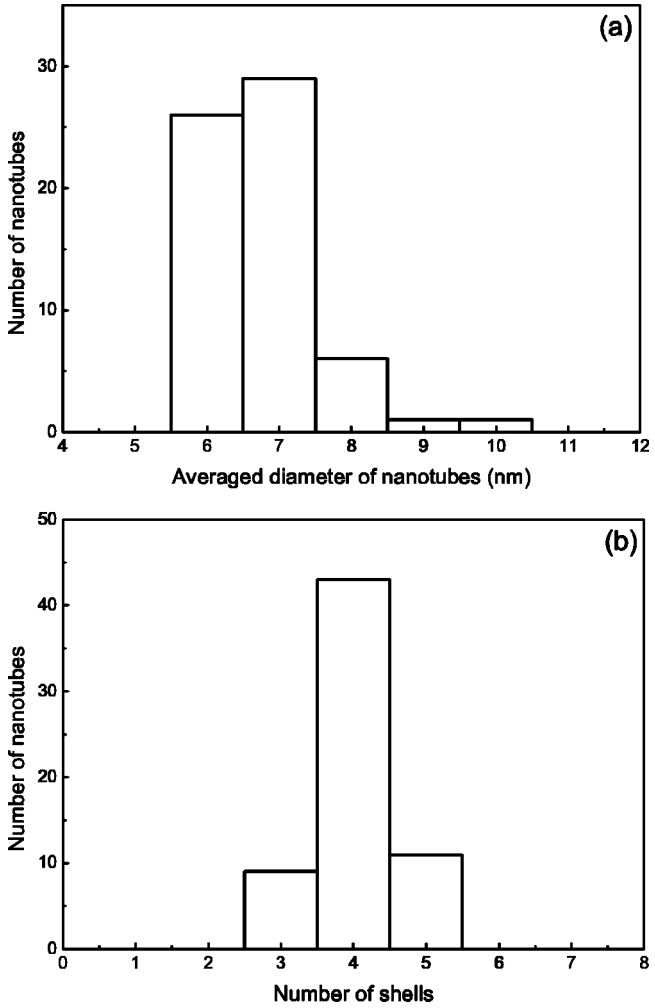

FIG. 3. Histograms showing respectively (a) the distribution of the averaged diameter and (b) the distribution of the number of shells of multiwall $H_2Ti_3O_7$ nanotubes.

1, and eventually roll into nanotubes with uniform diameters. In this paper we will be concerned mainly with the formation of the $H_2Ti_3O_7$-type nanotubes; in particular we would like to investigate what drives the formation of the $H_2Ti_3O_7$ nanotube from a flat $H_2Ti_3O_7$ plate, what determines the diameter, and the number of shells of the nanotube by the aid of first-principle calculations. A short summary on some of the results presented here may be found in Ref. 13.

II. COMPUTATION

Accurate *ab initio* calculations presented in this paper for either $Na_2Ti_3O_7$ or $H_2Ti_3O_7$ structures are based on the density functional theory (DFT) and performed using the CASTEP computer code[14] implemented in Cerius[2] software[15] and ultrasoft pseudopotentials.[16] The plane-wave basis was set with 300-eV kinetic energy cutoff. Exchange and correlation effects were included through the generalized gradient approximation,[17] and the Brillouin zone of the unit cell was sampled via a $3\times7\times3$ mesh.[18] The validity of the cutoff energy and mesh density was inferred from test calculations

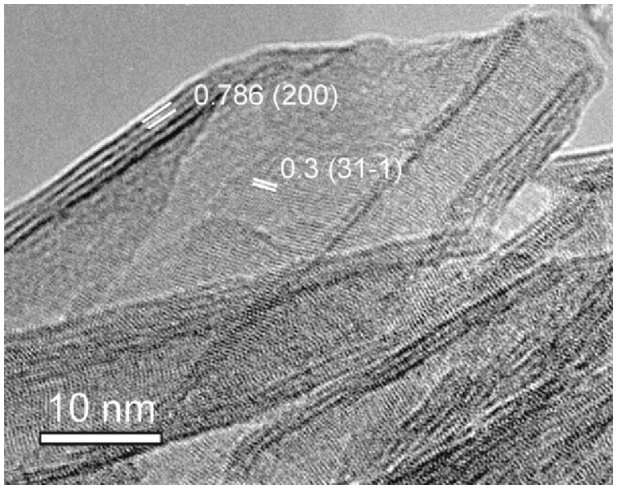

FIG. 4. High-resolution electron microcope image showing $H_2Ti_3O_7$ crystal plates and (200) and $(31\bar{3})$ lattice planes.

on anatase phase TiO_2 crystal. For this structure we obtained lattice constants $a=3.80$ Å and $c=9.89$ Å, in excellent agreement with experimental values[19] and recent first-principles FLAPW calculations.[20]

For nanotube calculations involving nearly one hundred atoms, self-consistent calculations are difficult to converge with the CASTEP method for configuration far away from the ground state. FASTSTRUCTURE code in CERIUS[2] software[15] was used to optimize the atomic configurations and calculate the total-energy values. FASTSTRUCTURE is an *ab initio* software package specifically designed to determine the structures of molecules, solids, and surfaces by calculating the energy and forces acting on the nuclei and determining the nuclear locations corresponding to the energy minimum. FASTSTRUCTURE is fast in comparison with other *ab initio* methods and yields results of comparable accuracy to these methods. It achieves its speed via algorithmic improvements (e.g., use of the so-called Harris functional[21] and a different optimization technique) and not via parametrization. The calculations used the local-density approximation (LDA) (Ref. 22) for the exchange-correlation potential and an energy cutoff of 300 eV.

III. RESULTS

A. Structures of $NaTi_3O_7$ and $H_2Ti_3O_7$

$Na_2Ti_3O_7$ and $H_2Ti_3O_7$ are two closely related structures. Experimentally single phase $NaTi_3O_7$ crystal may be obtained by mixing and heating stoichiometric quantities of dried $Na_2Ti_3O_7$ and TiO_2 (anatase) together at 1000 °C. $H_2Ti_3O_7$ crystal may be obtained by the method of ion exchange, i.e., exchanging interlayer Na^+ ions in $Na_2Ti_3O_7$ with H^+ by, e.g., immersing the powdered $Na_2Ti_3O_7$ in HCl aqueous solution for several days. The structure of $Na_2Ti_3O_7$ was determined by Andersson and Wadsley,[23] and the Ti-O framework of $D_2Ti_3O_7$ was given by Feist and Davis.[24] To obtain the atomic coordinates hydrogen ion positions we have performed *ab initio* structure optimization of these titanates starting from the model of Andersson and Wadsley[23]

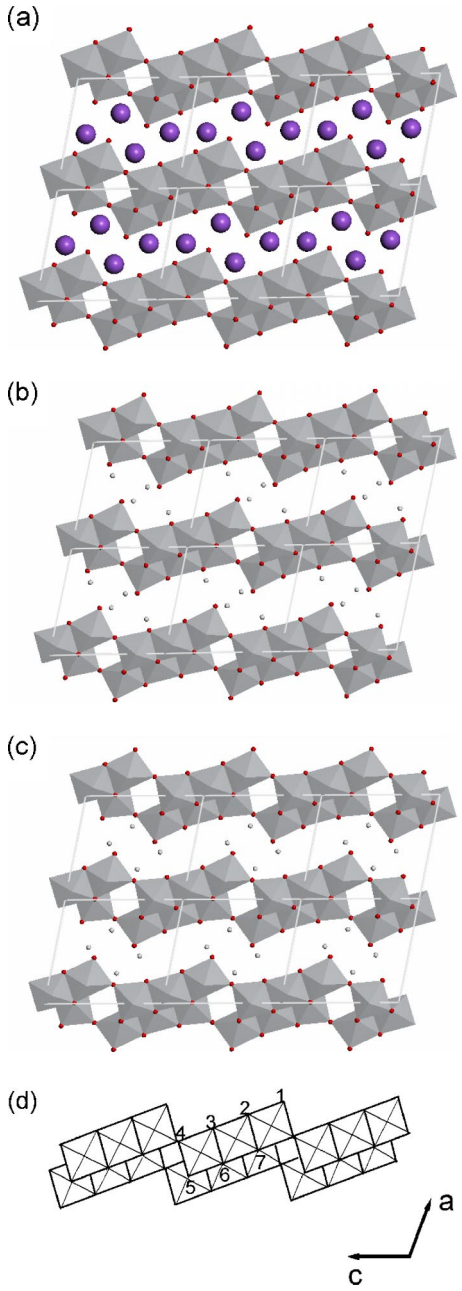

FIG. 5. Relaxed atomic configurations of (a) $Na_2Ti_3O_7$ and (b), (c) $H_2Ti_3O_7$. The $Na_2Ti_3O_7$ structure has a space group of $P21/M(11)$, and lattice parameters $a=8.740$ Å, $b=3.879$ Å, $c=9.320$ Å, $\beta=101.40^\circ$. For the structures of $H_2Ti_3O_7$ shown in (b) and (c) the space group is $P21/M(11)$ and lattice parameters are (b) $a=8.998$ Å, $b=3.764$ Å, $c=9.545$ Å, $\beta=102.65^\circ$ and (c) $a=8.771$ Å, $b=3.733$ Å, $c=9.759$ Å , $\beta=101.42^\circ$. In (d) is shown seven distinct oxygen sites for hydrogen absorption, and the atomic configuration shown in (b) and (c) correspond, respectively, to H(1,3) and H(1,4) to emphasize the fact that hydrogen atoms are absorbed at O1 and O3 sites in (b) and at O1 and O4 in (c).

and the optimized structures are shown in Fig. 5.

Figures 5(a)–5(c) show that the Ti-O skeleton of both $Na_2Ti_3O_7$ and $H_2Ti_3O_7$ consists of $[TiO_6]$ octahedrons, which share edges and corners. However, the positions of the interlayer H^+ and Na^+ ions are very different for the two

TABLE I. Energy per molecule for different configurations of hydrogen absorption.

	H(1,2)	H(1,3)	H(1,4)	H(1,5)	H(1,6)	H(1,7)
Energy (eV)	−7934.0	−7935.3	−7935.2	−7933.8	−7932.4	−7932.9

titanates. While the H-O bond length in $H_2Ti_3O_7$ is about 1 Å (which is very close to that in a H_2O molecule), the Na-O bond length in $Na_2Ti_3O_7$ is well above 2 Å. We therefore regard the H^+ ions as being adsorbed on the surface of the Ti-O skeleton while Na^+ being placed in the middle of the Ti-O layers. The O-O bond lengths of the $[TiO_6]$ octahedron are about 3 Å, and the short H-O bond with different oxygen sites results in very different total energies. Figure 5(d) shows that there exist seven distinct oxygen sites for hydrogen adsorption which we denote as O1, O2, etc. While O1 is bonded only with one Ti atom, O2, O3, O4 are bonded with two Ti atoms, O5 with three and O6, O7 with four Ti atoms, respectively. In a stoichiometric $H_2Ti_3O_7$ crystal two hydrogen atoms are bonded to these seven oxygen atoms, and in this paper we will refer to these configurations as H(i,j), where i and j denote, respectively, the two oxygen sites to which H atoms are bonded.

Full structural relaxation calculations were performed for different configurations H(i,j) with H^+ being adsorbed at different oxygen sites, and corresponding values of total energy per molecule were given in Table I. These values show that the capability of the different oxygen sites for adsorbing hydrogen is different resulting in different O-H bonding strength. While the O6-H bond is the weakest, the O1-H bond is the strongest. The minimum-energy configuration corresponds to two hydrogen atoms being adsorbed at the O1 and O3 sites, i.e., the H(1,3) configuration, and the next lowest configuration is the H(1,4) configuration having a total energy which is higher than that of the H(1,3) by 0.1 eV per molecule. The H(1,5), H(1,6), and H(1,7) configurations correspond to two H atoms being adsorbed on the opposite sides of the Ti_3O_7 crystal layer. The energies of these configurations are more than 1.0 eV higher than the lowest H(1,3) configuration. It should be noted that the energies of the H(1,4) and H(1,3) configurations are very close and it is therefore difficult to differentiate between the two configurations. In addition the total energy depends hardly on the space angle of the H-O bond associated with either O3 or O4 sites. This is perhaps the reason as to why the coordinates of hydrogen atoms are difficult to determine experimentally.[24] It was also noticed that after hydrogen absorption the corresponding Ti-O bond length was increased. This is because a certain amount of electrons were transferred from the Ti-O bond to the O-H bond as a result of the H^+ adsorption. The coupling energy between the layers, E_{coupl}, is 0.24 eV per molecule.

Listed in Tables II and III are atomic coordinates for a fully relaxed $Na_2Ti_3O_7$ structure compared with experimental values of Andersson and Wadsley,[22] and for fully relaxed H(1,3) and H(1,4) configurations of $H_2Ti_3O_7$ structures. The models shown in Figs. 5(a)–5(c) were constructed using the atomic coordinates given in these tables.

B. Formation of $H_2Ti_3O_7$ nanotubes

As briefly mentioned in the introduction, $H_2Ti_3O_7$-type nanotubes can be synthesized in a single alkali treatment.[10,11] Experimentally it was observed that these nanotubes have a diameter of about 6–8 nm and their lengths may range from 100 to several hundreds of nanometers. Extensive electron microscopy studies were carried out in order to elucidate the formation mechanism of these titanate nanotubes.[11] It was concluded that TiO_2 particles first reacted with NaOH solution to form a highly disordered intermediate phase containing Ti, O, and Na. Sheets of trititanate then started to extrude from the disordered phase and $H_2Ti_3O_7$ plates with several trititanate layers were formed. In what follows we consider mainly the formation of the nanotubes from these $H_2Ti_3O_7$ crystal plates.

We first consider how the NaOH solution environment affects the $H_2Ti_3O_7$ crystal plates. It should be noted that the concentration of Na^+ and OH^- in the interlayer region of a $H_2Ti_3O_7$ plate is much less than that in the NaOH solution. This means that the two sides of the surface layer of a $H_2Ti_3O_7$ crystal plate are in different chemical environments. The surface side of the layer is in direct contact with the solution and therefore is under much more frequent collisions by OH^- than the other side of the layer which is bounded to other layers beneath the surface layer. Our *ab initio* calculations show that the energy gain for an OH^- ion to carry away an absorbed H^+ on the surface is as large as 2 eV, it is therefore very likely that H^+ on the surface exposed in strong alkali solution will be neutralized by OH^- to form a water molecule. The hydrogen content on the two

TABLE II. Fractional atomic coordinates of $Na_2Ti_3O_7$ with a =8.7403 Å, b=3.8788 Å, c=9.3197 Å, α=90, β=101.3972, γ =90.0. All atoms in general positions for $P2_1/m$, $\pm x$, 0.25, z. Experimental values are taken from Andersson and Wadsley (Ref. 22).

Atom	x	x (expt)	z	z (expt)
Na	0.68047	0.682	0.59092	0.595
Na	0.50369	0.508	0.15580	0.154
Ti	0.03181	0.0278	0.27793	0.2806
Ti	0.24319	0.2467	0.67095	0.6730
Ti	0.14636	0.1420	0.98337	0.9811
O	0.21623	0.221	0.18323	0.195
O	0.14730	0.140	0.45902	0.473
O	0.43545	0.438	0.64935	0.645
O	0.32196	0.314	0.90835	0.885
O	1.01167	0.997	0.75148	0.745
O	0.80685	0.791	0.31710	0.313
O	0.91642	0.905	0.04532	0.031

TABLE III. Fractional atomic coordinates of $H_2Ti_3O_7$ with $a=8.998$ Å, $b=3.764$ Å, $c=9.545$ Å, $\alpha=90$, $\beta=102.654$, $\gamma=90.0$ for the H(1,3) configuration, $a=8.771$ Å, $b=3.733$ Å, $c=9.759$ Å, $\alpha=90$, $\beta=104.42$, $\gamma=90.0$ for the H(1,4) configuration. All atoms are in general positions for $P2_1/m$, $\pm x$, 0.25, z.

H(1,3)	x	z	H(1,4)	x	z
H	0.43642	0.54847	H	0.54270	0.72136
H	0.32474	0.22409	H	0.29267	0.44141
Ti	0.04261	0.29346	Ti	0.04498	0.27694
Ti	0.23795	0.67962	Ti	0.24864	0.70136
Ti	0.13965	0.96779	Ti	0.14685	0.98973
O	0.21704	0.17819	O	0.21276	0.17487
O	0.15456	0.46557	O	0.18343	0.44910
O	0.43353	0.64967	O	0.44193	0.65837
O	0.29712	0.88613	O	0.30472	0.88956
O	1.00780	0.75162	O	1.00846	0.75153
O	0.82956	0.32442	O	0.82970	0.32421
O	0.92343	0.05024	O	0.92089	0.04810

sides of the surface layer of a $H_2Ti_3O_7$ crystal plate is therefore not symmetric. The surface layer of the $H_2Ti_3O_7$ crystal will therefore be negatively charged by losing H^+ ions. The electrical neutrality is maintained by the positively charged Na^+ ions gathered near the surface. However, these Na^+ ions are only weakly bonded to the negatively charged Ti_3O_7 layer and in a way these ions may be regarded as a fluid of positive charge on the surface. While hydrogen atoms on the surface were frequently carried away by the colliding OH^- ions, it became more and more difficult for the hydrogen atoms to be taken away from the surface as more and more negative charges were accumulated on the surface. This is because these negative charges and the positive Na^+ ions gathered near the surface established a repulsive electric field and the strength of the field was proportional to the amount of negative charges accumulated on the surface. The limiting process preventing the runaway of the field strength is the reduction reaction of the Na^+ ions, i.e.,

$$Na^+ + e^- \rightarrow Na.$$

But this reduction half reaction has a standard potential of only -2.71V suggesting that the reaction is indeed a much slower process than that for a H^+ ion. As more and more negative charges were accumulated on the surface, the repulsive field became stronger and stronger. As a result it became more and more difficult for the OH^- ions to carry away hydrogen ions from the surface. On the other hand, as the field became stronger the reduction of Na^+ ions became easier and faster. Eventually an equilibrium between the two distinct processes was achieved resulting in a negatively charged surface layer with about 0.1 electron per molecule and a strong field of the order of 10^7V/M near the surface region. The degree of asymmetry in the hydrogen content on the two sides of the surface layer may be described by defining an average number of H^+ loss per molecule δ. While $\delta=0$ corresponds to a perfect stoichiometric $H_2Ti_3O_7$ surface layer, $\delta=1$ corresponds to a HTi_3O_7 layer without any hydrogen atoms on its surface side. As will be shown later, on average the surface is typically charged with less than 0.1 electron per molecule, while losing about 0.95 H^+ per molecule.

We mentioned in the preceding section that a bonded hydrogen will elongate the relevant O-Ti bond length. Conversely when H^+ ions are removed from the absorption sites the relevant Ti-O bonds on the surface will be contracted. Listed in Table IV are bond lengths of two Ti-O3 bonds for H(1,3) and H(1,4) configurations calculated using CASTEP. In this table we have used the notation that Ti(2,3) denotes the Ti atom having bonds with O2 and O3, and Ti(3,4) denotes that having bonds with O3 and O4. Changing from H(1,3) to H(1,4) configuration is equivalent to move a H atom from the O3 to O4 site, and as far as the Ti(2,3)-O3 and Ti(3,4)-O3 bonds are concerned the effect is that due to H desorption from the O3 site. Table IV shows that both Ti(2,3)-O3 and Ti(3,4)-O3 bonds are contracted after the H atom at the O3 site is removed.

The interlayer Na^+ ions and those gathered above the surface, on the other hand, have not much effect on the O-O-Ti bond lengths. This suggests that the surface layer of a $H_2Ti_3O_7$ plate will curve naturally if it is freed from the constraint of the layers beneath. We will show below that this effect indeed provides a sufficient driving force for the rolling of the surface layer from the rest of the crystal plate leading to the formation of the $H_2Ti_3O_7$-type nanotube.

C. Single-shell nanotube

A curved fragment of $H_{2-\delta}Ti_3O_7$ layer was constructed and the total energy of this fragment was calculated as a

TABLE IV. Calculated bond-length changes using CASTEP due to the H desorption from the O3 site.

Bond length (Å)	Ti(2,3)-O3	Ti(3,4)-O3
H(1,3)	1.948	2.050
H(1,4)	1.796	1.847
Changes	−0.152	−0.203

TABLE V. Calculated bond-length changes using FASTSTRUCTURE due to the H desorption from the O3 site.

Bond length (Å)	Ti(2,3)-O3	Ti(3,4)-O3
H(1,3)	1.979	1.999
H(1,4)	1.803	1.840
Changes	−0.176	−0.159

function of the radius of curvature or radius of the corresponding tube. Shown in Fig. 6(a) is such a relaxed fragment with $\delta=1.0$, where all H^+ ions adsorbed on the surface side were assumed to have been taken away by colliding OH^- ions in the NaOH solution. Although the real $H_{2-\delta}Ti_3O_7$ surface layer was slightly charged, in what follows we assume that the presence of a small amount of charges on the surface does not affect the equilibrium radius of curvature of the resultant nanotubes. Detailed local density-of-states calculations show that these charges are largely localized at the O1 and O2 sites [see Fig. 5(d)]. While the H-O1 bonds hardly affect the surface tension energy E_t that is responsible for the formation of the nanotube, H-O2 bonds hardly exist on the surface due to the exceedingly high energy (see Table I) compared with other hydrogen desorption configurations, e.g., H(1,3) and H(1,4). To a good approximation the driving force for the formation of the nanotube results mainly from the desorption of the hydrogen ions from the O3 sites, and finite net charges on the O1 and O2 sites are therefore neglected in our following calculations.

The fragment used in our calculations was assumed to be electrically neutral and composed of eight molecules of $H_{2-\delta}Ti_3O_7$. All electrons were included in the FASTSTRUCTURE *ab initio* calculations with the maximum relaxation step size being set at 0.01 bohr to obtain the metastable equilibrium position which preserves the curvature of the initial configuration. The geometry optimization calculation was terminated when forces on all atoms were smaller than 0.001 Ha/bohr. The FASTSTRUCTURE calculations were compared with the more expensive CASTEP calculations under the same conditions, i.e., LDA and a cutoff energy of 300 eV. The difference between the optimal lattice constants of the perfect $H_2Ti_3O_7$ crystal obtained using the two methods, i.e., CASTEP and FASTSTRUCTURE, was shown to be within 1.5%. For the most relevant Ti-O3 bonds in the H(1,3) and H(1,4) configurations, it was shown (see Tables IV and V) that the difference between the calculated Ti-O3 bond lengths ranges from less than 1% to 2.5% which is much less than the change of about 9% of the same bond length due to hydrogen adsorption and desorption. The use of the FASTSTRUCTURE method is therefore justified for investigating the effect of relevant Ti-O bond shortening on the formation of the nanotube.

Shown in Fig. 6(b) is the total-energy values plotted against the radius of curvature of the $H_{2-\delta}Ti_3O_7$ fragment. It should be noted that the structure toward the edges of the finite fragment is distorted when compared with that of the central part. But this distortion is localized around the edges and is basically the same for different fragments with different curvatures, we expect therefore that this distortion will

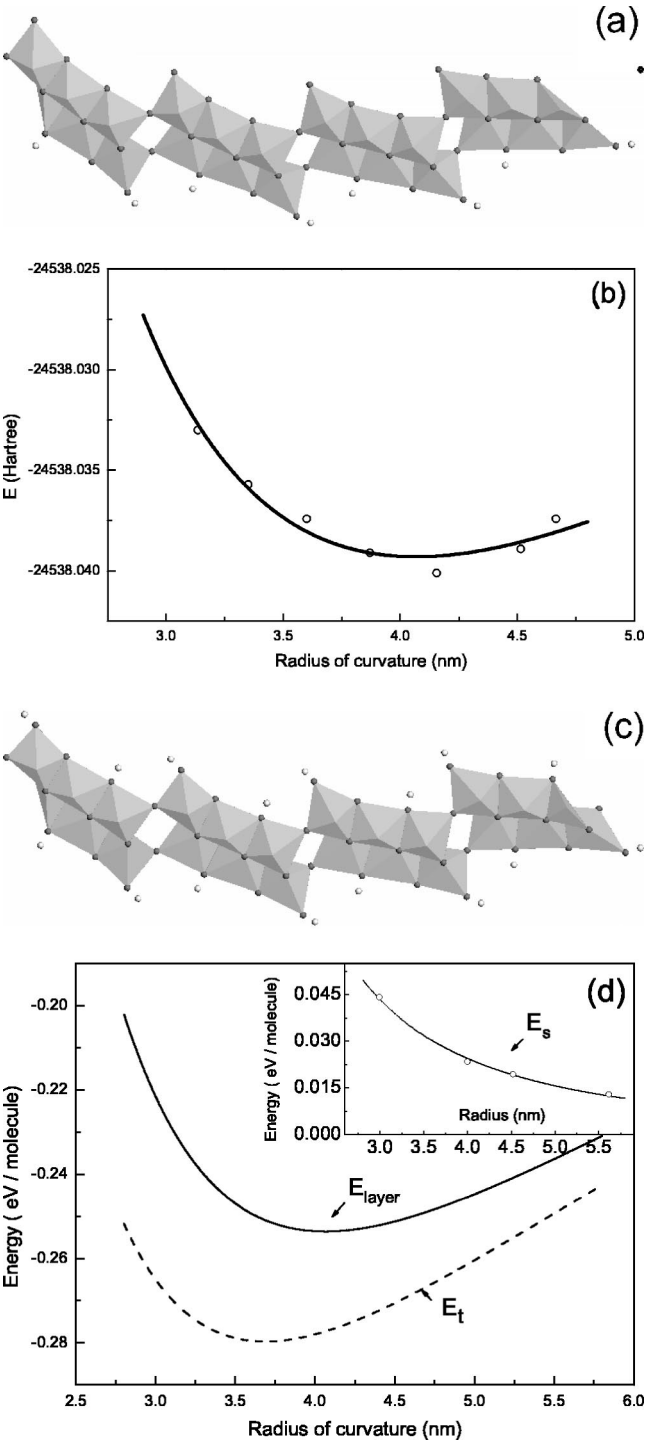

FIG. 6. (a) A relaxed curved fragment of a layer of $H_{2-\delta}Ti_3O_7$ crystal with $\delta=1.0$. The radius of curvature of the $H_{2-\delta}Ti_3O_7$ fragment is set so that the corresponding tube radius would be $R=4.16$ nm. (b) The total energy of a curved $H_{2-\delta}Ti_3O_7$ fragment as a function of the radius of curvature. The circles represent numerical results while the solid line is the fitted curve using the functional form $E_{\text{layer}}=\alpha/r^2-\beta/r+\gamma$. (c) A curved $H_2Ti_3O_7$ fragment and a radius of curvature $R=4.0$ nm. (d) The strain energy E_s, the surface tension energy E_t, and the total energy of a crystal layer E_{layer}, as a function of the radius of curvature ($\delta=1$).

not affect our final conclusions regarding the dependence of the total energy on the curvature.

The curve in Fig. 6(b) shows a clear minimum at ~4.0 nm, suggesting that there exists a nature curvature or corresponding tube radius R_0 around 4.0 nm which minimizes the total energy of the hydrogen deficient $H_{2-\delta}Ti_3O_7$ layer with $\delta=1$. This energy minimum results from two competing factors. The first factor is the strain energy resulting from the distortion of all bond lengths and angles when the crystal layer is bent, and this energy is against the bend of the $H_2Ti_3O_7$ crystal layer. Using a continuum elastic model the strain energy of a bent $H_2Ti_3O_7$ fragment may be written as

$$E_s = \frac{a}{R^2}, \tag{1}$$

where R is the radius of curvature of the bent fragment and a is a proportional constant.

The second factor is the surface tension energy resulting from hydrogen deficiency on the surface, and this energy favors the bending of the surface layer. As we mentioned in Sec. III A, on releasing a hydrogen atom from an oxygen site the relevant Ti-O bond will contract resulting in a surface tension which tends to bend the surface layer upward to release the surface tension. This surface-tension energy term may be written to a first-order approximation using the Hookes's law as

$$E_t = \frac{1}{2}\delta k(l-\delta l_0)^2, \tag{2}$$

where l represents the difference in the arc length of the two sides of the crystal layer averaged to one molecule, and δl_0 denotes the equilibrium value of l which reduces to zero when $\delta=0$. For a finite value of δ, the surface tension reduces to zero when $l=\delta l_0$. Equation (2) is derived using the superposition principle and assuming that the effective spring constant δk is proportional to hydrogen deficiency δ, which requires that the hydrogen vacancies on the surface do not interact strongly.

A simple geometric analysis reveals that l is inversely proportional to the radius of curvature of the layer R, i.e.,

$$l = \frac{c}{R}, \tag{3}$$

where c is a proportional constant. Let

$$R_0 \equiv \frac{c}{l_0}, \tag{4}$$

we then obtain

$$E_t = \frac{1}{2}\delta kc^2\left(\frac{1}{R}-\frac{\delta}{R_0}\right)^2 \equiv \delta b\left(\frac{1}{R}-\frac{\delta}{R_0}\right)^2, \tag{5}$$

with $b=(1/2)kc^2$. The total energy of the crystal layer is given by

$$E_{\text{layer}} = E_s + E_t + E_0 = \frac{a}{R^2} + b\delta\left(\frac{1}{R}-\frac{\delta}{R_0}\right)^2 + E_0, \tag{6}$$

where E_0 is the total energy per molecule for a perfectly flat $H_2Ti_3O_7$ crystal layer with $\delta=0$. This equation shows that the total energy for a curved crystal layer takes a functional form

$$E_{\text{layer}} = \frac{\alpha}{R^2} - \frac{\beta}{R} + \gamma, \tag{7}$$

on its dependence on R. We may therefore fit the numerical values of E_{layer} shown in Fig. 6(b) using this functional form to obtain $\alpha=1.233$ Ha nm^2, $\beta=0.607$ Ha nm and $\gamma=-24\,537.964\,71$ Ha. We may also arbitrarily set $E_{\text{layer}}=\gamma$ as the energy reference, i.e., the zero point, and use eV as the energy unit, the energy per molecule is then given by

$$E_{\text{layer}} = \frac{4.19}{R^2} - \frac{2.06}{R}, \tag{8}$$

and the corresponding curve E_{layer} shown in Fig. 6(d) was calculated using Eq. (8).

In general the parameters α and β depend on δ. To obtain the coefficients a, b, etc., that are independent of δ we note that the strain energy (1) is not very sensitive to the hydrogen content on the surface; to a good approximation we may therefore neglect the dependence of E_s on δ. A curved fragment of $H_2Ti_3O_7$ layer similar to that shown in Fig. 6(a) was then constructed and shown in Fig. 6(c). Since for this fragment we have $\delta=0$ and $E_t=0$, we can then calculate the total energy $E_{\text{layer}}=E_s+E_0$ as a function of R. When subtracted from E_0 we obtain the $E_s(R)$ curve which may be fitted as shown in the inset of Fig. 6(d) by

$$E_s = \frac{0.39}{R^2}, \tag{9}$$

which gives $a=0.39$ eV nm^2, $b=(\alpha-a)/\delta=3.80$ eV nm^2, and $R_0=2b\delta^2/\beta=3.69$ nm.

To extract the strain energy E_s due to bending from the total energy E_{layer} and thus to obtain the surface tension energy E_t resulting from hydrogen desorption from the surface, we made calculations of the total energy for atomic models having different hydrogen deficiency δ [$\delta=1.0$ for Fig. 6(a) and $\delta=0.0$ for Fig. 6(c)]. This then raises a question as to whether or not the strain energy E_s depends on the hydrogen content of the surface layer and how that affects the total energy. Comparing Eq. (5)–(9) we see immediately that the surface strain energy $E_s=0.39/R^2$ is only about 10% of that due to the surface tension energy [see Eq. (5)]. In principle the surface strain energy E_s due to the bending of the surface layer may be dependent on the hydrogen content of the layer, but this effect is small in comparison with that due to the surface tension resulting from the relevant Ti-O bonds shortening after H desorption from the corresponding O sites. We estimate that the error introduced by the approximation that E_s is independent of the hydrogen deficiency δ is much less than about 10% of the corresponding surface tension energy E_t.

The energy of a flat surface layer (with $R=\infty$) of a $H_2Ti_3O_7$ crystal will increase when the H^+ ions adsorbed on the surface are carried away by OH^- following Eq. (6),

$$\Delta E = \frac{b\delta^3}{R_0^2} = 0.28\delta^3. \tag{10}$$

By neglecting the effects of temperature and defects, we expect that the surface layer of a $H_2Ti_3O_7$ crystal plate will begin to break away from the bulk layers beneath when the coupling between them can no longer offset the energy increase due to the hydrogen deficiency on the surface, i.e., the criterion for the peeling of the surface layer from the crystal plate may be written as

$$\Delta E = E_{coupl}, \tag{11}$$

where E_{coupl} is the corresponding layer coupling energy. In general E_{coupl} is not a constant, and peeling would initiate at any place having minimum E_{coupl}. Since a $H_2Ti_3O_7$ crystal plate is composed of identical layers of atoms, peeling may occur anywhere in the crystal plate. It should be noted that locally the layer coupling energy E_{coupl} may be affected by many factors, e.g., local defects, and it is this fluctuation that provides the sites for the peeling process to initiate. Figure 4 shows that crystal layers may bend together around the edges of the crystal plates, and the number of layers bending together varies from 2 to 4.

In principle the coupling energy of the surface layer depends on the hydrogen deficiency on the surface. However, detailed calculations revealed that E_{coupl} is not sensitive to δ and to a good approximation we may use $E_{coupl}=0.24$ eV per molecule for our estimation as obtained for a perfect $H_2Ti_3O_7$ crystal plate. Using this value we obtain from Eq. (10) a critical value of $\delta=0.95$ for the peeling of the surface layer from a $H_2Ti_3O_7$ plate.

We mentioned briefly in our previous discussion on the effect of charges on the radius of the nanotube that different hydrogen atoms at different oxygen sites may have a different effect on the surface tension. In particular, the surface tension is hardly dependent on the hydrogen atoms bonded at the O1 sites, while that at the O3 sites are much more influencing. Shown in Figs. 7(a)–7(c) are three models of a curved fragment of a layer of $H_{2-\delta}Ti_3O_7$ with the same hydrogen deficiency $\delta=0.5$ but different radius of curvature [3.0 nm for Fig. 7(a), 4.1 nm for Fig. 7(b), and 5.5 nm for Fig. 7(c)]. Total-energy calculations for these models are performed and results are shown in Fig. 7(d) (circles) and fitted using the analytical functional form (7) with $\alpha=0.794$ Ha nm^2, $\beta=0.381$ Ha nm, and $\gamma=-24\,540.8961$ Ha. The optimum radius of curvature of the minimum energy is seen to be at 4.0 nm which is almost the same as that shown in Figs. 6(b) and 6(d). Although on average the total energy is expected to depend sensitively on the hydrogen deficiency δ of the surface layer, see, e.g. Eq. (6), the coincidence of the optimal radius of curvature for models shown in Fig. 6(a) with $\delta=1.0$ and Fig. 7 with $\delta=0.5$ suggests that microscopically the adsorption and desorption of H atoms at O1 sites [Figs. 7(a)–7(c)] hardly have any effect on the radius of optimum curvature. Microscopically the surface-tension energy

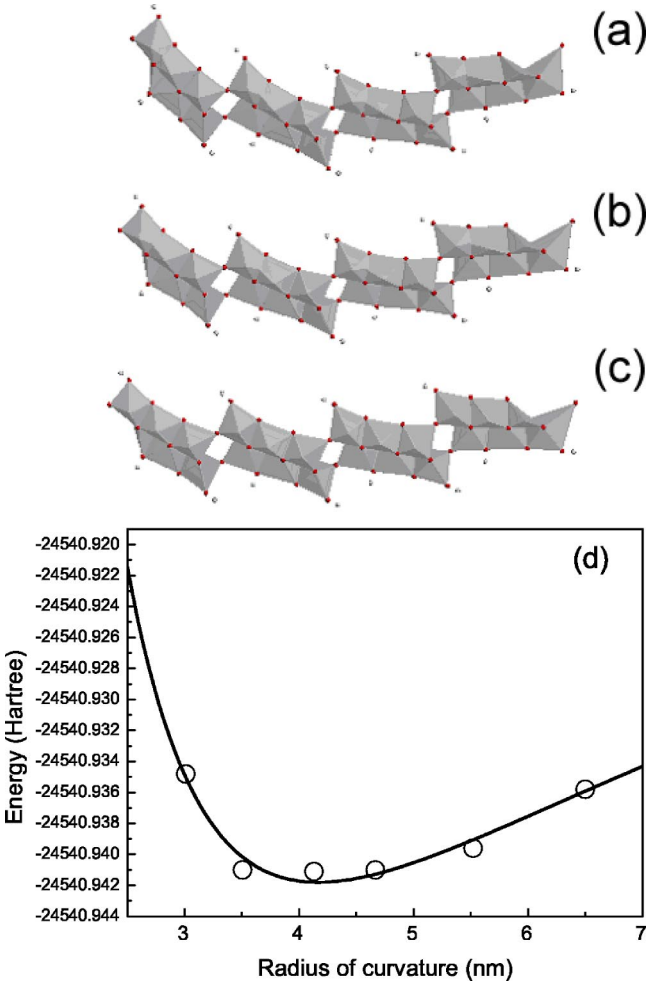

FIG. 7. A relaxed curved fragment of a layer of $H_{2-\delta}Ti_3O_7$ crystal with $\delta=0.5$ and a radius of curvature of (a) $R=3.0$ nm, (b) $R=4.1$ nm, and (c) $R=5.5$ nm. Shown in (d) are the calculated total energy (circles) of the curved $H_{2-\delta}Ti_3O_7$ fragment as a function of the radius of curvature and fitted curve using $E=\alpha/r^2-\beta/r+\gamma$.

and the optimal radius of curvature are determined mainly by the H atoms associated with the O3 sites, and hydrogen absorptions at other oxygen sites rarely occur due to the much higher energy (see Table I).

The optimized radius for a peeled surface layer may be obtained by minimizing the total energy with respect to R,

$$\frac{\partial E_{layer}}{\partial R} = 0, \tag{12}$$

giving

$$\bar{R} = \frac{2\alpha}{\beta} = \frac{(a+b\delta)R_0}{b\delta^2}. \tag{13}$$

Substitution of the known values of a, b, R_0 and δ into the above expression gives $\bar{R}_0=4.30$ nm, and this value agrees well with experimental results presented in Fig. 3.

Alternatively the radius can be expressed in terms of the coupling energy E_{coupl} using Eq. (10) and (11),

$$\bar{R} = \frac{(a + \delta b)}{\sqrt{\delta b E_{coupl}}}, \tag{14}$$

i.e., $\bar{R}$ is determined mainly by E_{coup}.

Although the peeling process may initiate for a surface layer with any number of layer n, only the layer with $n=1$ will continue the peeling process and roll into a tube. Figure 4 shows that although surface layers with $n>1$ may start to peel off or bend at the edges, the process cannot continue since the driving force due to surface hydrogen deficiency is just sufficient to overcome the layer coupling but not enough to compensate for the extra strain introduced by bending additional layers together. This conclusion is consistent with the experimental observation that nanotubes with considerably larger radius, or that resulting from the bending of a surface layer with $n>1$, have never been observed.

We have so far assumed that the nanotube is formed by rolling the trititanate sheet along the [010] direction with a chiral vector along the [001] direction. For a nonzero chiral angle θ, the parameter ℓ defined in Eq. (2) should be replaced by $\ell \cos\theta$. To a good approximation we may assume that the strain energy term E_s is independent of the chiral angle θ and the total energy of the layer can then be written as[13]

$$E_{\text{layer}}(R,\theta) = \frac{a}{R^2} + b\delta\left(\frac{\cos\theta}{R} - \frac{\delta}{R_0}\right)^2 + E_0, \tag{15}$$

and it can be readily shown that the minimum energy corresponds to $\theta=0$ (see Fig. 4 of Ref. 13) and this is why experimentally most nanotubes were found with the tube axis pointing along the [010] direction.

D. Multishell nanotube

The analysis presented in the proceeding section for the tube radius applies only to the case when the tube has only a single shell. When more shells are formed additional factors need to be considered. The first factor is the coupling between different shells. In general this coupling E_{coupl} lowers the total energy of the system, and favors the formation of larger tubes with many shells. On the other hand, when rolling a charged Ti_3O_7 layer to form a multishell nanotube the electrostatic Coulomb energy E_C will evidently increase. It should also be noted that when more shells are formed some of these shells will have radius which are different from the optimal radius $\bar{R}$ derived above. For a tube with many shells, the inner shells will have radii which are less than $\bar{R}$ while outer shells will have radii which are larger than $\bar{R}$. The total energy curve shown in Fig. 6(b) shows that deviation from the optimal radius $\bar{R}$ will inevitably increase the total energy of the crystal layer E_{layer}, but it will be shown below that this energy increase is not sufficient to offset the energy gain via shell coupling and therefore to stop the rolling process. The energy gain from the coupling between different shells E_{coupl} may be offset by the Coulomb repulsive E_C which increases E_{layer} rapidly, leading to the breakdown of the rolling process and imposing an upper limit of the tube diameter.

We first consider the tube coupling energy E^t_{coupl}. This energy results basically from van de Waals force between the $H_2Ti_3O_7$ atomic layers and is responsible for bonding these layers together. Assuming that the circumference of the tube is L, the average number of shells may be estimated as

$$N \approx \frac{L}{2\pi R_0}, \tag{16}$$

R_0 being the radius of curvature of the optimal tube having zero surface tension, i.e., $E_t=0$. Since the outermost and innermost shells are not coupled to any other layers, we have then an approximate expression for the averaged tube coupling energy per molecule,

$$E^t_{coupl} \approx \frac{N-1}{N} E_{coupl}, \tag{17}$$

where E_{coupl} is the layer coupling energy per molecule for a flat crystal plate. Assuming that there exist on average x positive charges (due to, e.g., Na^+ ions) per molecule between the shells of a tube, the positively charged ions will enhance the shell coupling via electrostatic force among the positive Na^+ ions and the negatively charged Ti_3O_7 shells, giving a modified form for the tube coupling energy,

$$E^t_{coupl} \approx [x k_{coupl}(d) + E_{coupl}]\frac{N-1}{N}, \tag{18}$$

in which k_{coupl} is a coupling constant which depends on the shell spacing d [$\sim$7.8 Å (Ref. 12)]. As mentioned before, the layer coupling energy E_{coupl} is not sensitive to the hydrogen deficiency δ, and to a good approximation we may assume $E_{coupl}=0.24$ eV per molecule as for a perfect $H_2Ti_3O_7$ crystal. The main effect due to the finite residual charge on the surface layer is taken in account by the Coulomb repulsive energy E_C.

The Coulomb repulsive energy E_C results from the fact that when a hydrogen deficient $H_2Ti_3O_7$ layer rolls into a tube, the tube is negatively charged. It should be noted that the hydrogen deficient surface layer of $H_2Ti_3O_7$ is only slightly charged. The negative charge left by the hydrogen atoms being carried away by the colliding OH^- ions may be compensated partially by the exchange of electrons with surrounding Na^+ ions and also by the existence of oxygen vacancies. The rate for the surface charging and discharging processes are, however, very different, and basically the balance is determined by the much slower process of electron exchange between the positively charged Na^+ and the negatively charged $H_2Ti_3O_7$ surface layer. The net result is that there remains a residual charge on the surface.

By assuming that there exist equal amount of positively charged Na^+ ions inside the innermost shell and outside the outermost shell of the nanotube, moving one half of the negative ions inside the tube inward and the other half outward to the innermost and outermost surfaces respectively, and utilizing the Gauss theorem, we may write an approximate expression for this energy $E_C(N)$,

$$E_C(1) = 0,$$

$$E_C(2) = 0,$$

$$E_C(3) = k_C\rho^2 r_0^2 \ln\left(\frac{r_0+d}{r_0-d}\right),$$

$$E_C(4) = 4k_C\rho^2\left[(r_0+0.5d)^2\ln\left(\frac{r_0+1.5d}{r_0+0.5d}\right) + (r_0 - 0.5d)^2\ln\left(\frac{r_0-0.5d}{r_0-1.5d}\right)\right],$$

$$E_C(5) = k_C\rho^2\left\{r_0^2\ln\left(\frac{r_0+d}{r_0-d}\right) + [r_0+2(r_0+d)]^2\ln\left(\frac{r_0+2d}{r_0+d}\right) + [r_0+2(r_0-d)]^2\ln\left(\frac{r_0-d}{r_0-2d}\right)\right\}, \quad (19)$$

in which

$$k_C = \frac{\pi e^2}{n\epsilon_0 b^2 c^2} = 0.11 \text{ eV/Å}^2, \quad (20)$$

where n is the number of molecules in the tube of unit length, r_0 is the averaged radius of tube, ρ is the average number of Na^+ ions per molecule existing outside the outermost shell and inside the innermost shell, and d is the spacing between shells.

In the limit of $r_0 >> d$ we have

$$E_C(1) = 0,$$

$$E_C(2) = 0,$$

$$E_C(3) = 2k_C\rho^2 r_0 d,$$

$$E_C(N) = E_C(N-2) + (N-2)^2\, E_C(3). \quad (21)$$

The important point to note here is that E_C increases rapidly with increasing number of shells, and terms which are proportional to N^2 are involved. The Coulomb energy is also seen to be proportional to both r_0 and d resulting in a force of contraction on both the radius of the tube and the shell spacing, and this explains why the experimentally observed shell spacing ($\sim$0.78 nm) of the nanotube is smaller than that of its bulk counterpart ($\sim$0.88 nm).

For a multishell nanotube, the radius of curvature of the tube is not a constant but a monotonically increasing function from inner shells to outer shells. The deviation of the curvature from that which minimizes the layer energy,

$$E_{layer}(\bar{R}) = \frac{\alpha}{\bar{R}^2} - \frac{\beta}{\bar{R}} + \gamma, \quad (22)$$

may be calculated via

$$E_R = \int E_{\text{layer}}(R)ds/L - E_{\text{layer}}(\bar{R}), \quad (23)$$

where the integration should be performed along the intersecting contour of the multishell tube with a perpendicular plane from the innermost shell to the outermost shell, and L is the total length of this contour. Experimentally it was found that the $H_2Ti_3O_7$-type nanotubes have typically four shells [see Fig. 3(b)], we may therefore neglect the dependence of E_R on the number of shells and write this energy term only as a function of the tube radius R, i.e., $E_R(R,\delta)$, where the dependence on δ comes via the dependence of the constants β and γ on δ.

The increase in the total energy for a multishell nanotube may be written as

$$\Delta E_t \approx E_C(\rho,d,N) - E^t_{\text{coupl}}(x,d,N) + E_R(\delta,R). \quad (24)$$

It should be noted that the energy term E_R alone is not sufficient to offset the energy gain E^t_{coupl} due to shell coupling, i.e., for a neutral nanotube the rolling process would not terminate and the resulting tube will inevitably have a large size distribution which is determined mainly by the size of the $H_2Ti_3O_7$ crystal plates from which the tubes were formed. Figure 3(b) shows, however, that this is not the case. There exist a relatively sharp peak in the histogram of the shell number N. This result strongly suggests that the Coulomb energy term E_C plays an important role in the determination of the diameter and shell number of the tube, i.e. the tube is charged with ρ.

For a charged nanotube, the shell number N is determined mainly by the competition between energy gain due to shell coupling E^t_{coupl} and energy increase in E_C. For a small nanotube the total tube energy is overweighted by the coupling energy E^t_{coupl} and this energy gain drives the rolling process to proceed. On the other hand as the tube becomes bigger and the tube number N increases, the positive Coulomb energy E_C increases more rapidly with N than the tube coupling energy E^t_{coupl} and eventually it becomes unfavorable for the rolling process to continue. Since E_R is not sensitive to the shell number N, we may neglect this term in deriving the following condition for the rolling crystal sheet to break or the rolling process to stop

$$E_C - E^t_{coupl} \gtrsim E_b, \quad (25)$$

in which E_b is related to the potential barrier for the breaking of the layer ($\sim$0.2–0.3 eV). The above argument also suggests that the outer diameter of the tube is determined largely by the E_{layer} term since E_b results mainly from a local barrier and does not depend explicitly on R_{out}. Assuming r_0 = 4.3 nm, d = 0.78 nm, a simple estimation gives $E_C(4)$ = 0.2 eV/molecule and $\rho \sim 0.026$, i.e., there exists approximately only 0.026 Na^+ ion per molecule near the outmost and inner most shell of the tube.

E. Stability of the multiwalled nanotube

Following our earlier arguments on the formation of the nanotube one may have noticed that as soon as the surface $H_{0.95}Ti_3O_7$ layer starts curling, its underside surface gets exposed to the alkaline environment and would undergo similar bond-shortening when losing hydrogen as that of the top surface before the curling. One would guess that the driving force for the curling would then stop and the curled $H_{0.95}Ti_3O_7$ layer would lose its curvature. But this is not true. While it is true that as soon as the underside surface of the $H_{0.95}Ti_3O_7$ layer gets exposed to OH^- ions it will lose hydrogen, this process is a slow process comparing with the

curling process. This is because the curling surface layer is negatively charged and the repulsive field substantially reduced the rate at which hydrogen ions were carried away from the curling layer by the OH^- ions. The multiwalled nanotube may be formed and surface tension released rapidly once the surface layer breaks from the beneath layers without losing much hydrogen to the alkaline environment. Since the surface $H_{0.95}Ti_3O_7$ layer is charged, a much stronger electric field than that of the $H_{0.95}Ti_3O_7$ plate would be established in the space between the newly exposed outermost shell of the nanotube and the positively charged Na^+ ions gathered near the shell. This stronger electric field will reduce substantially the hydrogen desorption rate from the outermost shell. In principle, most of the hydrogen atoms on the outermost shell of the nanotube will eventually be lost to the alkaline environment, thus losing driving force for the curling. A curved symmetric Ti_3O_7 layer would tend to become flat to reduce the strain energy E_s as given in Eq. (7). But this energy of about 0.02 eV is much smaller than the shell coupling energy E^t_{coupl} of about 0.18 eV for $N=4$. Basically the nanotube is protected by the strong shell coupling from becoming flat again.

IV. CONCLUSIONS

In summary, we have proposed a mechanism for the formation of $H_2Ti_3O_7$-type nanotubes from $H_2Ti_3O_7$ plates. Although a perfect $H_2Ti_3O_7$ plate has a symmetric layered structure, when placed in an alkali solution the chemical environment becomes different for the two sides of the surface layer of the crystal plate resulting in an asymmetry in its hydrogen content on the two sides of the surface layer. We have shown via first-principle *ab initio* calculations that it is this hydrogen distribution asymmetry on the two sides of the surface layer that provides a necessary and sufficient driving force for the peeling of the surface layer and the formation of the $H_2Ti_3O_7$-type nanotubes of uniform diameter after the surface layer is freed from the beneath layers. We have shown that the radius of the rolled nanotube is determined mainly by the coupling energy between the rolling surface layer and beneath layers; the wall thickness or number of shells of the rolled nanotube is determined both by the layer coupling energy and residual charges on the rolling surface layer.

ACKNOWLEDGMENTS

The authors would like to thank Professor R. S. Han, Dr. G. H. Du, Dr. K. Y. Shi, J. J. Chao, B. L. Wang, and F. Lin for their help and stimulating discussions. This work was supported by the Ministry of Science and Technology (Grant No. 001CB610502), National Science Foundation of China (Grant Nos. 90206021 and 60401013), the Key Project (Grant No. 10401) of the Chinese Ministry of Education, National Center for Nanoscience and Technology, China, and Peking University.

*Author to whom correspondence should be addressed. E-mail address: Impeng@pku.edu.cn

[1] S. Iijima, Nature (London) **354**, 56 (1991).
[2] N. G. Chopra, R. J. Luyken, K. Cherry, and V. H. Crespi, Science **269**, 966 (1995).
[3] Z. Weng-sieh, K. Cherrey, N. G. Chopra, and X. Blase, Phys. Rev. B **51**, 11 229 (1995).
[4] R. Tenne, L. Margulis, and M. Genut, Nature (London) **360**, 444 (1992).
[5] Y. Feldman, E. Wasserman, and D. A. Srolovitz, Science **267**, 222 (1995).
[6] W. K. Hsu, Y. Q. Zhu, C. B. Boothroyd, I. Kinloch, S. Trasobares, H. Terrones, N. Grobert, M. Terrones, R. Escudero, G. Z. Chen, C. Colliex, A. H. Windle, D. J. Fray, H. W. Kroto, and D. R. M. Walton, Chem. Mater. **12**, 3541 (2000).
[7] M. Niederberger, H. J. Muhr, F. Krumeich, F. Bieri, D. Gunther, and R. Nesper, Chem. Mater. **12**, 1995 (2000).
[8] T. Kasuga, M. Hiramatsu, and A. Hoson, Langmuir **14**, 3160 (1998).
[9] T. Kasuga, M. Hiramatsu, A. Hoson, T. Sekinio, and K. Niihara, Adv. Mater. (Weinheim, Ger.) **11**, 1307 (1999).
[10] G. H. Du, Q. Chen, and L.-M. Peng, Appl. Phys. Lett. **79**, 3702 (2001).
[11] Q. Chen, W. Zhou, G. H. Du, and L.-M. Peng, Adv. Mater. (Weinheim, Ger.) **17**, 1208 (2002).
[12] Q. Chen, G. H. Du, S. Zhang, and L.-M. Peng, Acta Crystallogr., Sect. B: Struct. Sci. **52**, 587 (2002).
[13] S. Zhang, L.-M. Peng, Q. Chen, G. H. Du, G. Dawson, and W. Z. Zhou, Phys. Rev. Lett. **91**, 256103 (2003).
[14] M. C. Payne, M. P. Teter, D. C. Allan, T. A. Arias, and J. D. Joannopoulos, Rev. Mod. Phys. **64**, 1045 (1992).
[15] Accelry http://www/accelrys.com/cerius2/
[16] D. Vanderbilt, Phys. Rev. B **41**, 7892 (1990).
[17] B. Hammer, L. B. Hansen, and J. K. Norskov, Phys. Rev. B **59**, 7413 (1999).
[18] H. J. Monkhorst and J. D. Pack, Phys. Rev. B **13**, 5188 (1976).
[19] J. K. Burdett, T. Hughbanks, G. J. Miller, J. W. Richardson, Jr., and J. V. Smith, J. Am. Chem. Soc. **109**, 3639 (1987).
[20] R. Asahi, Y. Taga, W. Mannstadt, and A. J. Freeman, Phys. Rev. B **61**, 7459 (2000).
[21] J. Harris, Phys. Rev. B **31**, 1770 (1985).
[22] S. J. Vosko, L. Wilk, and M. Nusair, Can. J. Phys. **58**, 1200 (1980).
[23] S. Andersson and A. D. Wadsley, Acta Crystallogr. **14**, 1245 (1961).
[24] T. P. Feist and P. K. Davis, J. Solid State Chem. **101**, 275 (1992).